Electronic Supplementary Material (ESI) for Lab on a Chip.

Supplemental Information

Flow-induced fabrication of ZnO nanostructures in pillar-arrayed microchannels

Ruyi Xu[1], Siyu Li[1], Sai-Xi Yu[2], Yan-Jun Liu[2], Wenhui Xie[1], Qingfeng Zhan[1], Zhenjie Zhao[1*], Xin Li[1*]

1 Engineering Research Center for Nanophotonics and Advanced Instrument, School of Physics and Electronic Science, East China Normal University, Shanghai 200062, China

2 Shanghai Institute of Cardiovascular Diseases, Shanghai Key Laboratory of Medical Epigenetics, International Co-laboratory of Medical Epigenetics and Metabolism (Ministry of Science and Technology), Institutes of Biomedical Sciences, Zhongshan Hospital, Fudan University, Shanghai 200032, China.

Corresponding authors:

zjzhao@phy.ecnu.edu.cn (Zhenjie Zhao)

xli@phy.ecnu.edu.cn (Xin Li)

1. Numerical analysis

a. Stokes equation[1]

According to the principle of momentum conservation, the motion of a fluid satisfies the Navier-Stokes (N-S) equations. Which is given by:

$$\rho\frac{\partial V}{\partial t}+\rho(V\cdot\nabla)V=-\nabla p+\mu\nabla^2V-\frac{2}{3}\nabla(\mu\nabla\cdot V)+\rho f_v \text{ * MERGEFORMAT (1)}$$

In this equation, the contributions of fluid acceleration, pressure gradient, viscous forces, and volume forces are considered. Here, ρ represents the density of the fluid, V represents the velocity vector of the fluid, p represents the pressure, μ represents the dynamic viscosity, and f_v represents the volume force per unit mass.

In microfluidic chips, the fluid is typically treated as an incompressible, isotropic Newtonian fluid, and the flow is often characterized by low Reynolds numbers in a steady or quasi-steady state. Under these conditions, the inertial forces and nonlinear terms was neglected, and thus the Stokes equation can be expressed as:

$$0=-\nabla p+v\nabla^2V \qquad \text{* MERGEFORMAT (2)}$$

b. Reynolds number (Re)[2]

The Reynolds Number (Re) is a dimensionless parameter that illustrates stationary incompressible fluid flows characterized by a single spatial scale L, which can be expressed as:

$$Re=\frac{UL}{\eta} \qquad \text{* MERGEFORMAT (3)}$$

where U is the characteristic velocity of the fluid, η is its kinematic viscosity of the fluid, L is the hydraulic diameter of channel, given by $\frac{2wh}{w+h}$ (h is the height and w is

the width of the channel).

c. Shear stress and shear rate[3]

Shear stress is used to describe the force per unit area parallel to the flow direction in a fluid when it undergoes deformation or shear. The fluidic shear stress τ is calculated using the formula:

$$\tau = \mu \frac{\partial u}{\partial y} \qquad \text{* MERGEFORMAT (4)}$$

where u is the flow velocity along the microchannel, and y is the distance from the nearest channel wall to the point inside the fluid, perpendicular to the direction of flow. The shear rate $\partial u / \partial y$ represents the rate at which adjacent layers of fluid move with respect to each other. Typically, the dilute solution of water is regarded as a Newtonian fluid, characterized by a unique property where shear stress is directly proportional to shear rate. Consequently, with an increase in shear rate, there is a corresponding increase in shear stress with a constant known as viscosity (μ).

d. Stagnant layer[4]

With the growth of the nanowires, they consume the growth units from the precursor solution and a stagnant layer is formed between the top nanowire surfaces and the area in the precursor solution at the distance δ. In the laminar regime, this boundary thickness can be estimated using the following expression:

$$\delta(x) \cong 5\sqrt{\frac{\eta x}{u}} \qquad \text{* MERGEFORMAT (5)}$$

where u is the velocity of fluid flow, x is the distance from the leading edge of the pillar, η is its kinematic viscosity of the fluid. The presence of a stagnant layer

resulted in gradient concentration of solute, impacting the crystal growth process. In microfluidic chips, mass transfer relied on diffusion within the stagnant layer. Increasing the flow rate can reduce the stagnant layer, thus shortening the time for solute diffusion to the crystal surface and promoting crystal growth.[5]

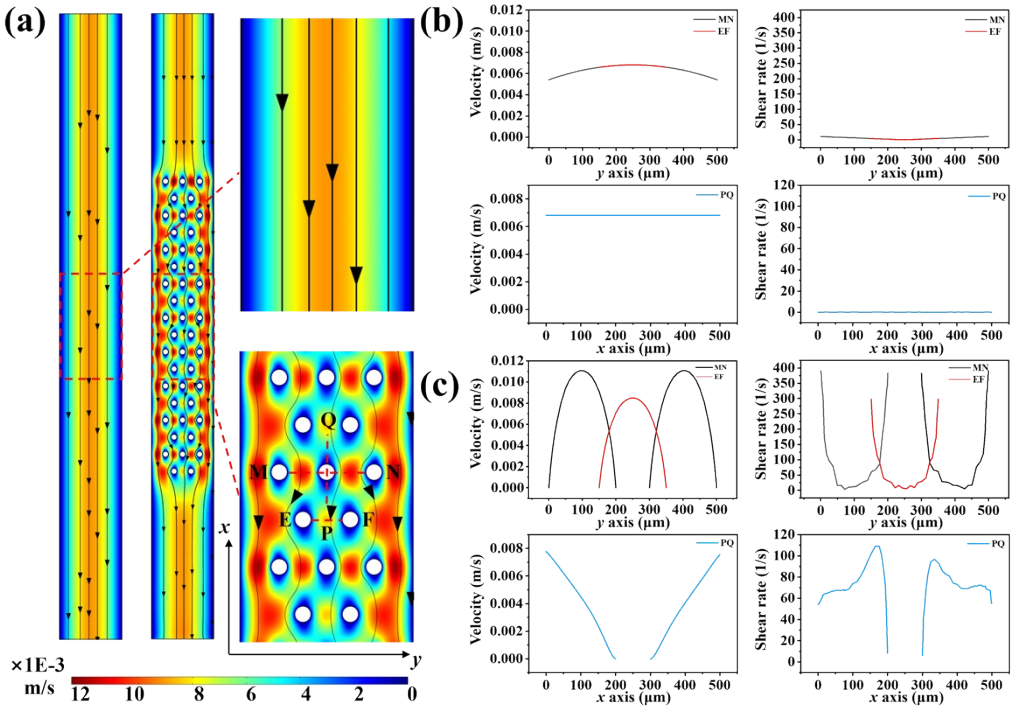

Figure S1. (a) Simulated velocity fields within microchannel with micropillar-arrays and without micropillar-arrays. (b) Corresponding profiles of flow velocity and shear rate in the channel without micropillar-arrays. (c) Corresponding profiles of flow velocity and shear rate in the channel with micropillar-arrays.

The distribution of flow fields in two-dimensional planes of different chip designs were shown in Fig. S1(a). The results indicated that compared to the straight microchannel, the addition of micropillar arrays regulated the local flow field distribution. To quantitatively described the characteristics of the flow, we investigated the velocity and shear rate distribution different along three lines (MN, EF, and PQ) in the two types of microchannels, as shown in the Fig. S1(b-c). The

flow direction (PQ direction) is defined as the *x*-axis, and the direction perpendicular to the flow direction (MN and EF direction) is the *y*-axis.

The simulation results indicated that the straight channel exhibited a parabolic Poiseuille flow with relatively uniform shear stress distribution perpendicular to the flow direction, accompanied by velocity changes from 0.005 m/s to 0.007 m/s and shear rate variations from 0 to 12 /s. Along the flow directions, a constant flow velocity of 0.007 m/s with a shear rate of 0 was observed. However, in the channel featuring micropillar arrays, the flow field distribution underwent significant variation. Perpendicular to the flow direction, the presence of micropillars induced multiple parabolic flow field profiles. It led to elevated local flow velocities between the micropillars and a dramatic reduction in flow velocity near their edges, resulting in a variation of flow velocity between 0 and 0.011 m/s. The shear stress variation exhibited a roughly parabolic trend and ranges from 0 to 380/s. Along the flow velocity direction, flow velocity experienced a sudden drop in the proximity of the pillars, thus the shear stress initially increased and then decreased. The velocity changed from 0 m/s to 0.008 m/s and shear rate varied from 10 to 110 /s.

2. Analysis of ZnO nanostructures prepared in the microchannels

The seed layer on glass substrate was investigated by AFM to reveal the influence of seeding layer preparation conditions on ZnO nanowires, as shown in Fig. S3. It can be observed that smaller seed crystals with a denser distribution were obtained with a flow rate of 5 μL/min, while larger seed crystals with a more uniform and dispersed distribution were obtained with a flow rate of 20 μL/min. It might be

attributed to the higher deposition rate of ZnO crystals at higher flow rates, which coalesced small grains into larger ones after annealing. Thus, lower seed density provided more space for precursor supply during growth, coupled with larger grain size, resulting in larger nanowire dimensions. It also reduced growth competition between nanowires, leading to significant difference of growth rate and broader size distributions.

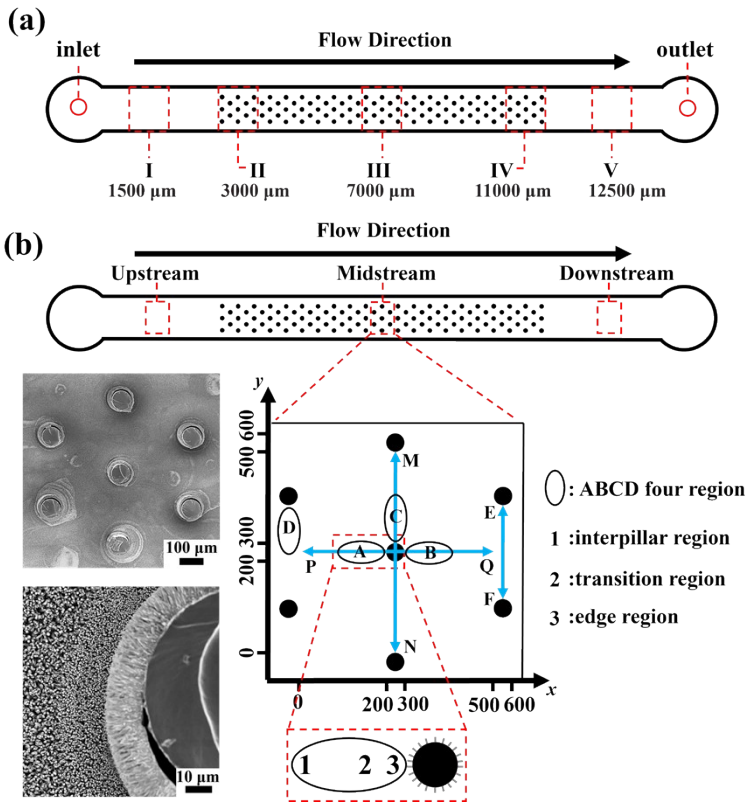

Figure S2. Schematic of microchannel structure and flow regions in the microchannels.

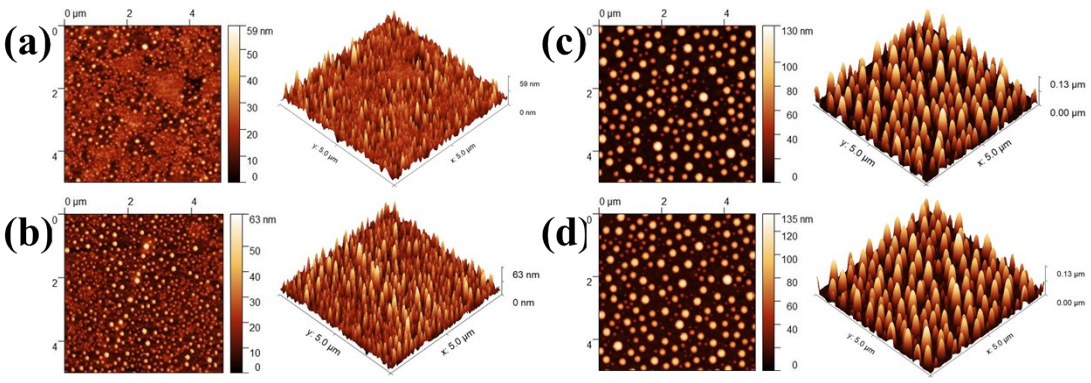

Figure S3. AFM images under different preparation conditions of seeding layer (a) UF-5 (b) BF-5

(c) UF-20 (d) BF-20

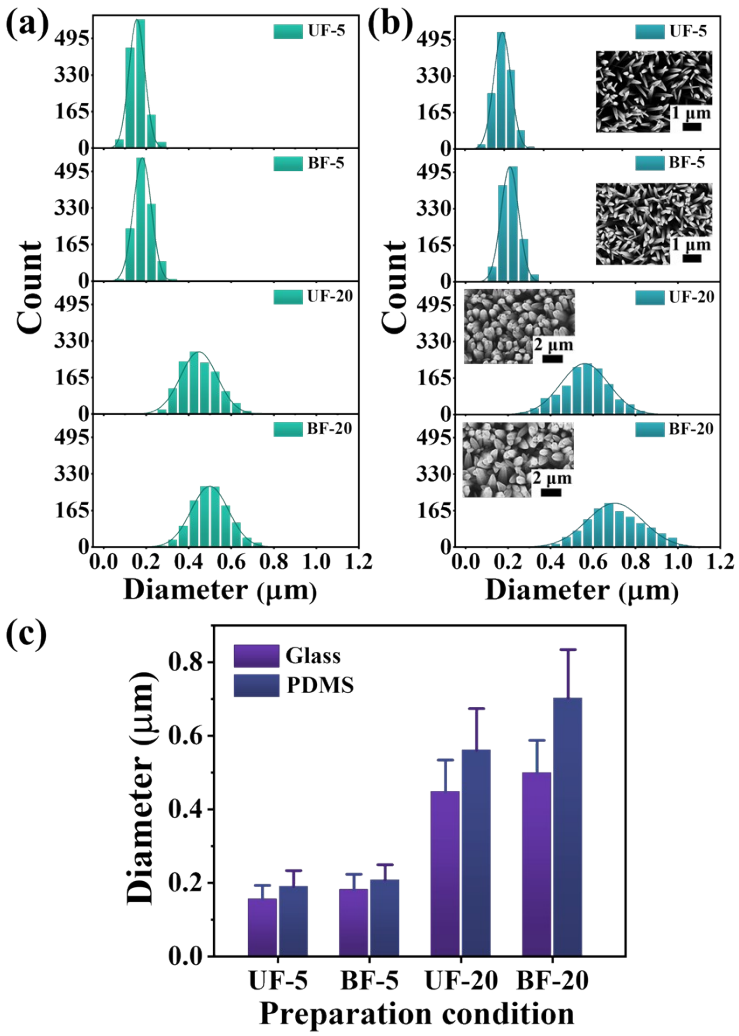

Figure S4. Diameter distribution of ZnO nanowires grown on the glass (a) and PDMS (b) substrate under different preparation conditions of the seed layer. (c) A bar graph showing the diameter of nanowires grown on the different substrates in the microchannels. ($N = 5$)

Although seeding layers with lower flow rates had higher densities, the formation of smaller nuclei due to smaller crystals might impede the radial and axial growth of a single ZnO nanowire. Furthermore, the consumption of the ZnO nanocrystals gradually decreased along the flow direction, leading to a gradual decrease in crystal deposition and a significant accumulation of crystals in the upstream region. UF promoted the heterogeneous nucleation along the flow direction,

resulting in thinner seeding layer crystals in the midstream region, while BF reduced this effect, resulting in a relatively thicker "pre-formed" seeding layer, leading to slightly higher diameters, lengths, and aspect ratios of ZnO nanomaterials in the BF mode compared to the UF mode.

We examined the crystallinity of the nanowires with different morphologies synthesized under each preparation condition of the seeding layer. Fig. S5 revealed that all ZnO nanowires exhibited a hexagonal wurtzite crystal structure. Significantly, the diffraction peak intensity of the (002) plane was found to be the highest, indicating a preferential growth orientation of the ZnO nanowires along the *c*-axis direction. In addition, ZnO nanowires grown on PDMS substrates displayed lower peak intensities, indicating a comparatively weaker degree of orientation in comparison to those grown on glass substrates.

To primarily reveal the impact of pillar arrays on the growth of ZnO nanomaterials, we studied the morphology variation along the front and back of the pillars for the sample of ZnO-UF-20 and ZnO-BF-20 (Fig. S6). The results showed that the diameter of ZnO at the leading edge of the pillars slightly larger than that at the trailing edge of the pillar. This is primarily due to a significantly higher concentration of Zn^{2+} ions in the leading-edge region of the pillar compared to the trailing-edge region. Notably, the UF mode resulted in a significant difference in the diameter of nanowires grown on the leading edges and trailing edges, while the BF mode reduced this effect. The change in fluid flow direction led to a different distribution of crystals in the channel, and the continuous flow in the opposite

direction served as a buffer to reduce the nonuniform distribution of crystals in the seeding layer.

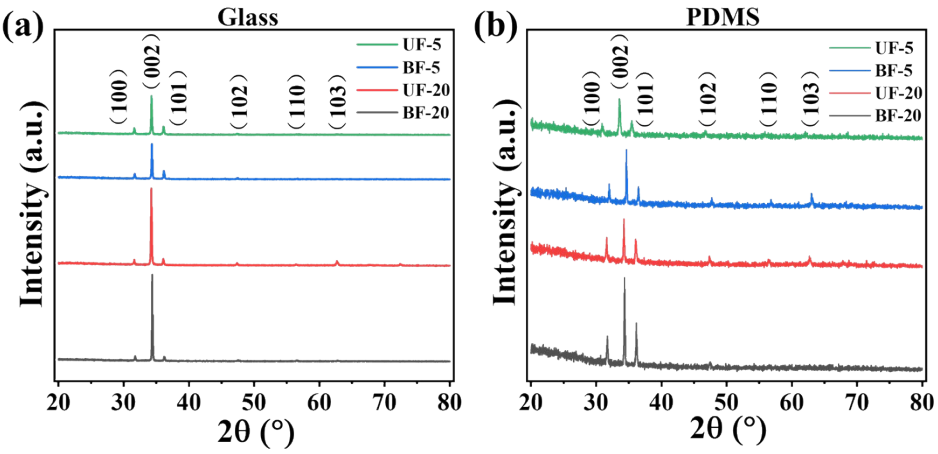

Figure S5. XRD pattern of ZnO nanowires grown on the glasses (a) and PDMS (b) under different seed layer condition.

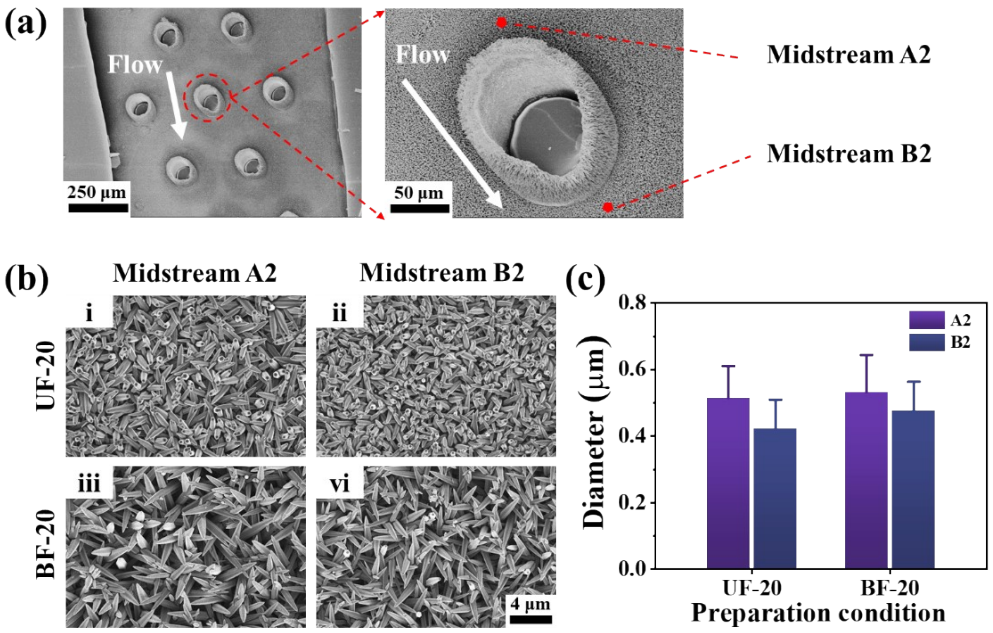

Figure S6. (a) SEM images of microchannel with micropillar arrays after synthesis of ZnO nanomaterials. (b) SEM images of ZnO nanowires grown in the leading-edge region A2 and trailing-edge region B2 under UF-20/BF-20 condition. (c) Corresponding bar graph of the diameter of ZnO nanowires. ($N = 4$)

Table1. Surface area per square micrometer of ZnO nanowires grown under different preparation conditions of the seed layer.

Preparation Condition	Density (μm^{-2})	Length (μm)	Diameter (μm)	Surface area (μm^2)
unidirectional flow, 5 μL/min (UF-5)	5.14±0.807	5.58±0.527	0.16±0.037	14.17
bidirectional flow, 5 μL/min (BF-5)	4.90±0.847	6.57±0.844	0.18±0.042	18.51
unidirectional flow, 20 μL/min (UF-20)	3.50±0.769	13.2±1.217	0.45±0.086	65.48
bidirectional flow, 20 μL/min (BF-20)	2.59±0.621	16.31±0.919	050±0.088	71.45

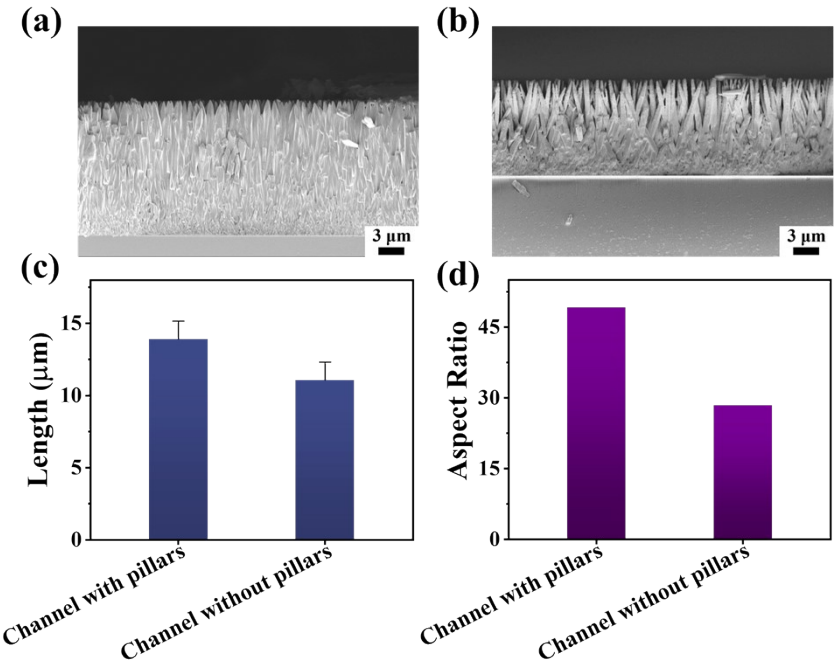

Figure S7. Morphology of ZnO nanostructures grown in midstream. Cross-sectional SEM images of ZnO nanowires prepared in the microchannel with micropillar-arrays (a) and without micropillar-arrays (b). (c) Corresponding bar graph of the length of ZnO nanowires. (d) Corresponding bar graph of the aspect ratio of ZnO nanowires. All aspect ratios were calculated by dividing the average length of ZnO nanowires by the average diameter. ($N = 4$)

Fig. S8 shows how the concentration of Zn^{2+} evolved in the channel with time. The corresponding diffusion time scale ($T_{diff} = L^{\wedge}2/D$)[6] is approximately 9 s with the

flow rate of 15 μL/min, where L is the characteristic length and D is the diffusion coefficient. The simulation results suggested that Zn^{2+} diffused throughout the entire channel in an extremely short time and initiated the reaction. As the reaction occurred downstream, fewer Zn^{2+} were available in the solution, leading to a decrease in their concentration in the middle and downstream regions. This, in turn, affected the growth of ZnO nanowires, resulting in variations in diameter and density along the flow direction.

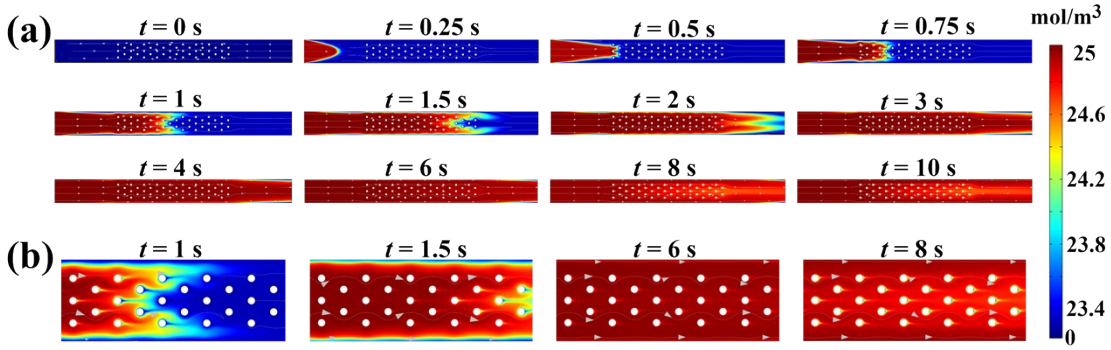

Figure S8. (a) Concentration variation of Zn^{2+} as a function of reaction time in the simplified channel (concentrations increase from blue to red). (b) Magnified images taken at t=1 s, 1.5 s, 6 s and 8 s.

TEM investigation of ZnO nanowires grown in the microchannel with pillars is shown in Fig. S10 (a). It can be clearly seen that in the HRTEM image, the fringes are perpendicular to the wire axis and the space between the adjacent planes is close to 0.52 nm, indicating that the crystalline ZnO nanowires grow along the [002] direction. Elemental mapping analysis was also conducted to determine the elemental distribution of the nanowires. The observed uniform distribution of the two elements confirmed the formation of ZnO crystals (Fig. S10 (b)). XRD patterns of ZnO nanowires grown in the midstream region with each reaction time are shown in Fig.

S10 (c). For each sample, XRD of nanowires showed typical wurtzite structure with (002) preferred orientation and the highest peak was observed at the reaction time of 2 h.

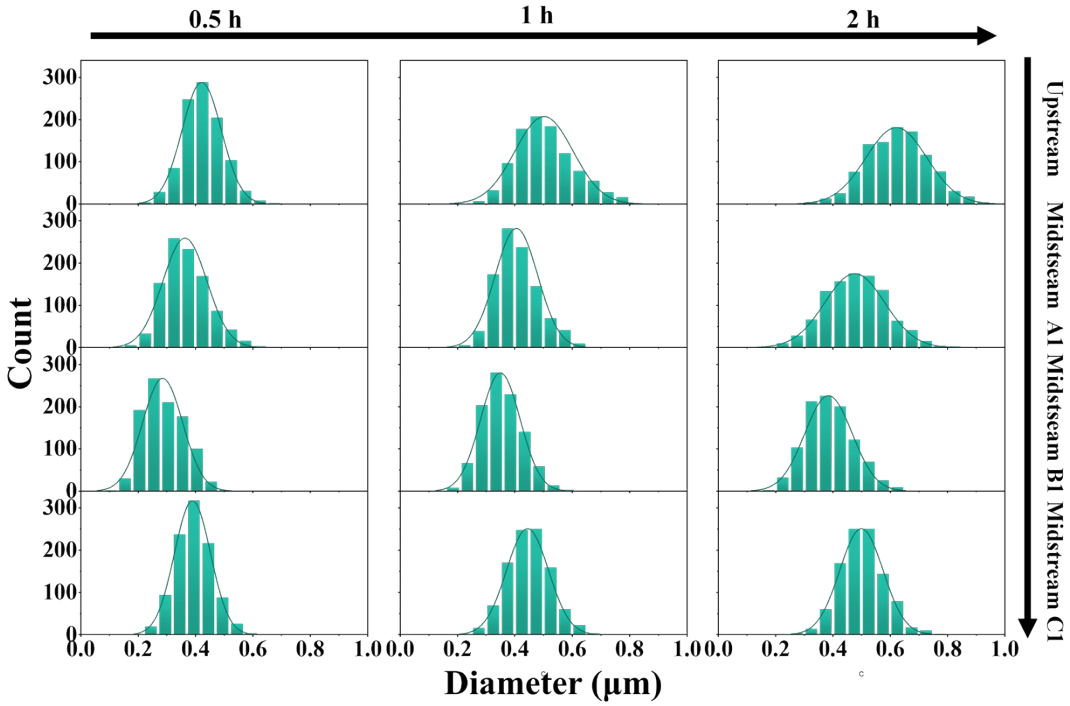

Figure S9. Diameter distribution of ZnO nanowires grown for 0.5 h, 1 2h and 2 h in the different four regions. ($N = 4$)

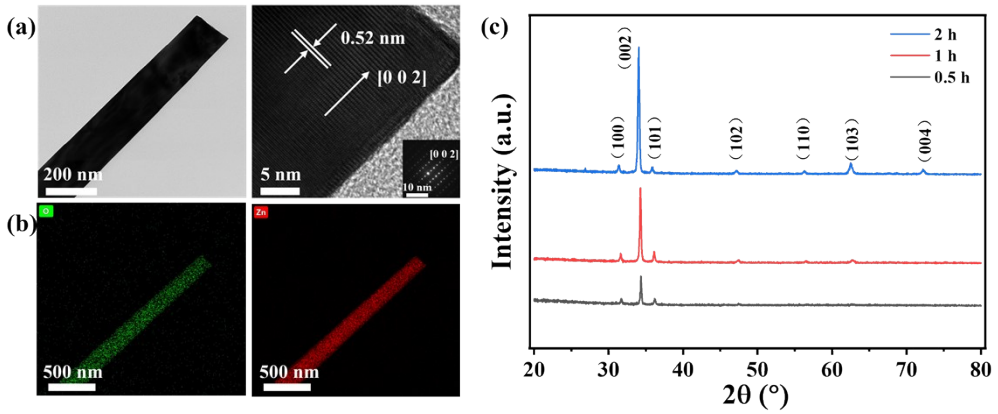

Figure S10. (a) TEM image (the left panels) of ZnO nanowires grown for 2 h in the microchannel with micropillar arrays, HRTEM image (the right panels) and the corresponding selected-area electron diffraction (SAED) pattern (insert). (b) EDS elemental mapping images of the ZnO nanowires grown for 2 h. (c) XRD pattern of ZnO nanowires grown for 0.5 h, 1 h and 2 h.

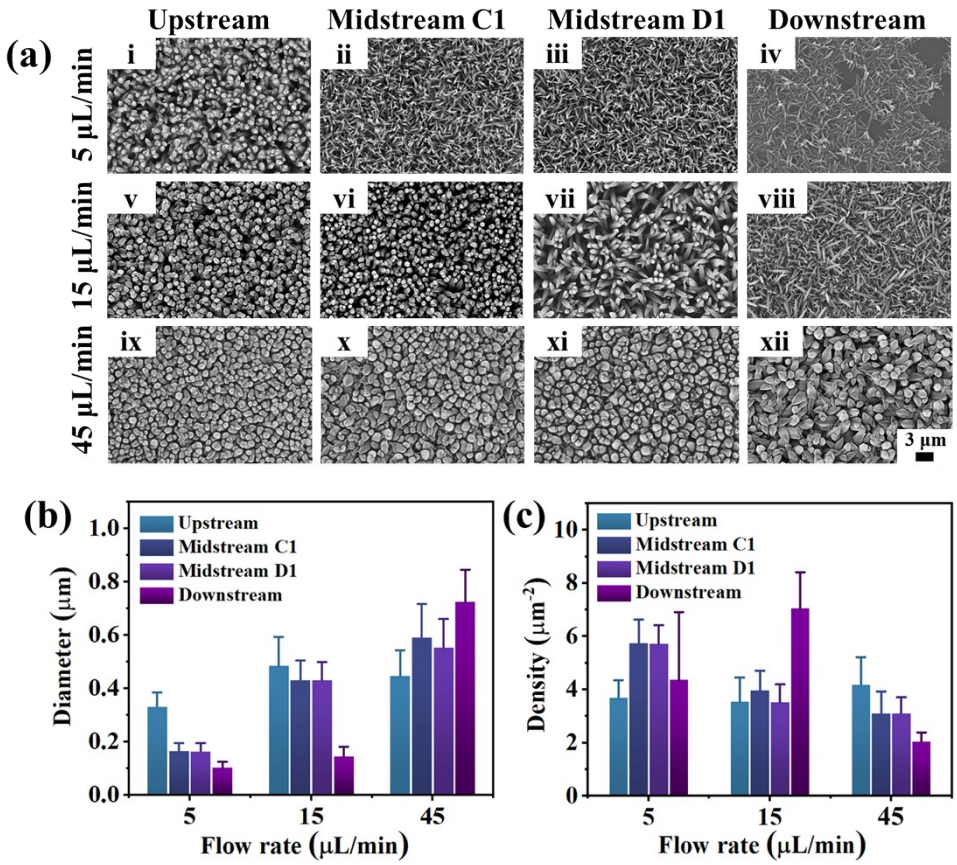

Figure S11 (a) Top-view SEM images of ZnO nanowires grown with the flow rates of 5, 15 and 45 μL/min in the four regions: ZnO nanowires grown for 5 μL/min (i), 15 μL/min (v) and 45 μL/min (ix) in the region of upstream; ZnO nanowires grown for 5 μL/min (ii), 15 μL/min (vi) and 45 μL/min (x) in the region of midstream C1; ZnO nanowires grown for 5 μL/min (iii), 15 μL/min (vii) and 45 μL/min (xi) in the region of midstream D1; ZnO nanowires grown for 5 μL/min (iv), 15 μL/min (viii) and 45 μL/min (xii) in the region of downstream. (b) A bar graph showing the corresponding diameter of nanowires. (c) A bar graph showing the corresponding density of nanowires. ($N = 4$)

In continuous flow synthesis, the flow rate can significantly affect the synthesis of ZnO nanomaterials. ZnO nanostructures were prepared at various flow rates of 5, 15 and 45 μL/min to investigate how flow rate tailors the morphology and size of the nanostructures. Accordingly, Reynolds numbers of the laminar flow were approximately 0.15, 0.44 and 1.32. As it can be seen lower flow rate (5 μL/min) resulted in larger difference of diameter of ZnO nanowires along the flow direction,

whereas a higher flow rate produced more uniform nanowires. The length of the nanowires increased slightly with a higher flow rate. In addition, the rapid growth of nanowires under higher flow rates led to evident fusion between the nanowires, further hindering the adsorption of fluorescent molecules, which was not beneficial to the further biodetection. Therefore, an optimal flow rate was identified as more suitable for fluorescence biodetection.

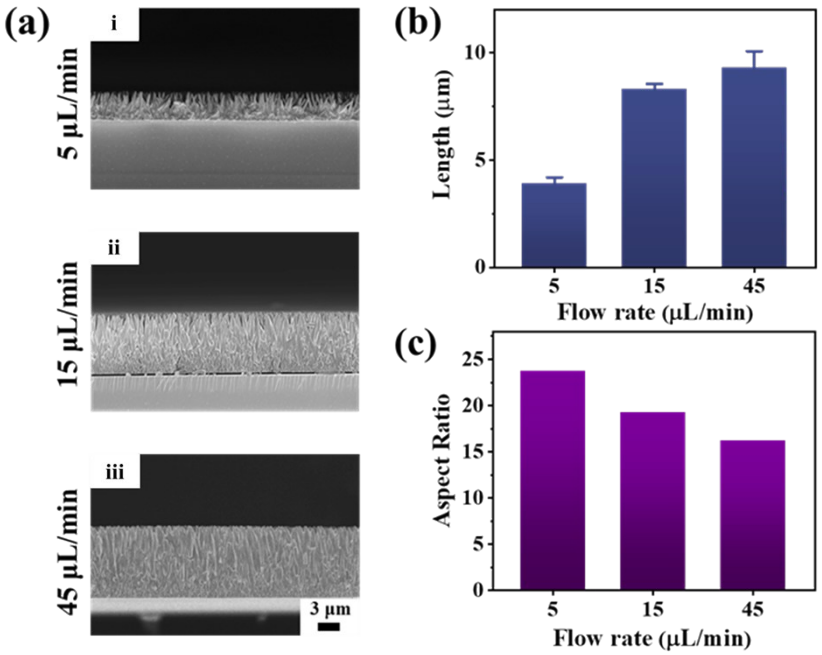

Figure S12 (a) Cross-sectional SEM images of ZnO nanowires grown with the flow rates of 5 μL/min (i), 15 μL/min (ii) and 45 μL/min (iii) in the midstream region. (b) A bar graphs showing the corresponding length of nanowires. (c) A bar graph showing the corresponding aspect ratio of nanowires. ($N = 4$)

Reference

1 P. K. Grzegorz Łukaszewicz, *Navier–Stokes Equations*, Springer, Switzerland, 2016.

2 T. M. a. Q. Squires, Stephen R., *Rev. Mod. Phys.*, 2005, **77**, 977-1026.

3 P. Tabeling, *Introduction to Microfluidics*, Oxford Academic, Oxford, 2023.

4 I. V. Markov, World Scientific, Singapore, 2003, pp. 170-190.

5 R. D. Sosa, X. Geng, M. A. Reynolds, J. D. Rimer and J. C. Conrad, *Lab on a Chip*, 2019, **19**, 1534-1544.

6 G. Wang, C. Yuan, B. Fu, L. He, E. Reichmanis, H. Wang, Q. Zhang and Y. Li, *ACS Applied Materials & Interfaces*, 2015, **7**, 21580-21588.